The synthesis and characterization of a xanthan gum-acrylamide-trimethylolpropane triglycidyl ether hydrogel

Meixia Zheng, Fengli Lian, Yao Xiong, Bo Liu, Yujing Zhu, Song Miao, Longtao Zhang, Baodong Zheng

PII: S0308-8146(18)31486-9
DOI: https://doi.org/10.1016/j.foodchem.2018.08.083
Reference: FOCH 23425

To appear in: *Food Chemistry*

Received Date: 27 January 2018
Revised Date: 28 July 2018
Accepted Date: 20 August 2018

Please cite this article as: Zheng, M., Lian, F., Xiong, Y., Liu, B., Zhu, Y., Miao, S., Zhang, L., Zheng, B., The synthesis and characterization of a xanthan gum-acrylamide-trimethylolpropane triglycidyl ether hydrogel, *Food Chemistry* (2018), doi: https://doi.org/10.1016/j.foodchem.2018.08.083

The synthesis and characterization of a xanthan gum-acrylamide-trimethylolpropane triglycidyl ether hydrogel

Meixia Zheng[#,a], Fengli Lian[#,b,c], Yao Xiong[b,c], Bo Liu[a], Yujing Zhu[a], Song Miao[c,d], Longtao Zhang[b,c,*], Baodong Zheng[b,c]

[a] *Agricultural Bio-Resources Research Institute, Fujian Academy of Agricultural Sciences, Fuzhou, Fujian 350003, PR China*

[b] *College of Food Science, Fujian Agriculture and Forestry University, Fuzhou, Fujian, PR China*

[c] *China-Ireland International Cooperation Laboratory of Foods Material Science and Structural Design, Fujian Agriculture and Forestry University, Fuzhou, Fujian, PR China*

[d] *Teagasc Food Research Centre, Moorepark, Fermoy, Co. Cork, Ireland*

[#] The authors contribute equally to this work.

* Corresponding authors: E-mail: zlongtao@fafu.edu.cn

ABSTRACT

To improve the thermal stability and adsorption performance, xanthan gum was modified with acrylamide and trimethylolpropane triglycidyl ether (TTE). The modified xanthan gum (XGTTE) was characterized by Fourier transform infrared (FT-IR) spectroscopy, X-ray diffractogram (XRD), differential scanning calorimetry (DSC) and scanning electron microscopy (SEM). The characteristic peaks at 3449, 1655, 1611 and 1420 cm^{-1} in the FT-IR confirm the modification. The XGTTE crystal grew well upon addition of TTE. The XRD and DSC data revealed that the XGTTE enhanced its thermal stability. Analysis of SEM revealed that the grafting introduced major changes on the microstructure making it porous and resulting in the adsorption of crystal violet (CV) with flocculation. The CV adsorption capacity of the hydrogel with different dosages of TTE (XGTTE2, XGTTE3, XGTTE4, XGTTE5 and XGTTE6) were between 28.13 with 35.12 mg/g. In addition, the adsorption capacity, thermal stability, and swelling property of XGTTE4 were the best.

Key word Xanthan gum, modification, Acrylamide, Trimethylolpropane triglycidyl ether

1. Introduction

Xanthan gum (XG) is a polysaccharide secreted by the bacterium *Xanthomonas campestris*. It primarily consists of a primary chain of β-D-(1, 4)-glucose, which has a branching trisaccharide side chain composed of β-D-(1,2)-mannose attached to β-D-(1, 4)-glucuronic acid, which terminates in a final β-D-mannose (Gils, Ray, & Sahoo, 2009). It is widely used as a food additive and rheology modifier and is commonly used in oral and topical formulations as a suspending and stabilizing agent and as a release sustaining agent in hydrophilic matrix tablets and pellets (Katzbauer, 1998). It is low cost, biodegradable, broadly available, and non-toxic (Bhardwaj, Kanwar, Lal, & Gupta, 2000).

There are many hydrophilic groups in the molecular chains of XG. Its property can be customized and extended by hybridization with synthetic polymers. Acrylic acid (Abhijit Pal, Majumder, & Bandyopadhyay, 2016), 2-acrylamido-2-methyl-1-propane sulfonic acid (Aflaki, Dadvand, & Sheykhan, 2016), ethylacrylate (Pandey & Mishra, 2011), acrylamide (AM) (Behari, Pandey, Kumar, & Taunk, 2001) and N-vinylpyrrolidone (Ding, Yiming, Yanjie, Bao, & Yongfu, 2016) have been grafted onto XG. The chemical amalgamation of natural and synthetic polymer resulted in a yield of new materials with superior properties.

AM is one of the most important grafting materials. Kumar et al. (2009) synthesized matrix XG-g-poly(AM) that could be used as drug delivery system with a fast release of the active substance (Kumar, Singh, & Ahuja, 2009). Behari et al. (2001) grafted AM onto XG to improve the thermal stability (Behari, Pandey, Kumar, &

Taunk, 2001). Biswas et al. (2015) reported the grafted copolymer XG-graft-poly(AM) could be used as a corrosion inhibitor (Biswas, Pal, & Udayabhanu, 2015). Mundargi et al. (2007) investigated the utilization of XG-grafted copolymer of AM as a controlled release matrix for antihypertensive drugs (Mundargi, Patil, & Aminabhavi, 2007). Trimethylolpropane triglycidyl ether (TTE) was used as a cross linking agent in the modification of macromolecule. Xiong et al. (2015) grafted sodium polyacrylate on guar gum and the polymers were then surface-crosslinked using TTE to improve its swollen property (Xiong, Zhang, & Liu, 2015). Huang et al. (2005) utilized TTE and acrylic acid to synthesize a novel photosensitive prepolymer (Huang, Wang, Liao, &Yuan, 2015). However, grafting AM and TTE on XG simultaneously had not been reported.

Aquatic products constitute a main part of food (Ashraf, 2005). According to the latest statistics released by the FAO (Food and Agriculture Organization) database, the global aquaculture is 110.2 million tons in 2016. Crystal violet (CV) is widely used as bacteriostatic agent in aquaculture (Mani & Bharagava, 2016). Moreover, CV can be detected from aquaculture water samples (Huang, Wang, Liao &Yuan, 2015) and processed fish products (Lee, Kim, Jang, Song, Woo, Park, Lee, Lee & Kim, 2010). CV is a toxic, genotoxic and carcinogenic substance (Mani & Bharagava, 2016), because of its toxicity, dye removal from aquaculture water and reducing residual dose in food is essential. Many approaches to the removal of CV have been studied including adsorption (Chen, Chen, Chiou, Chen, Chen, & Fan, 2011; Lin, He, Han, Tian, & Hu, 2011), photocatalytic degradation (Sahoo, Gupta, & Pal, 2005) and

biological methods (Chen, Chen, Chiou, Chen, Chen, & Fan, 2011; Lin, He, Han, Tian, & Hu, 2011), etc. Of these, adsorption seems to be the most promising (Aysu & Küçük, 2015; Mahdavinia, Aghaie, Sheykhloie, Vardini, & Etemadi, 2013; Monash & Pugazhenthi, 2009; Anjali Pal, Pan, & Saha, 2013).

This work is aimed to prepare a novel hydrogel base on AM and TTE grafted XG, for the first time. The modified XG was characterized by Fourier transform infrared (FT-IR) spectroscopy, X-ray diffraction (XRD), differential scanning calorimetry (DSC) and scanning electron micrograph (SEM). The effect of hydrogel for removal of CV from aqueous solution was studied. This finding might be contribute to reduce the CV pollution in aquaculture and improve food safety of aquatic products.

2. Experimental

2.1. Materials

Xanthan gum (XG, USP, PubChem CID: 7107) was purchased from Aladdin Industrial Corporation. The CAS is 11138-66-2, the molecular formula is $C_{35}H_{49}O_{29}$, and it is moisture sensitive. Acrylamide (AM, AR, 99.0%, PubChem CID: 6579; C_3H_5NO) was purchased with a molar mass of 71.08. Trimethylolpropane triglycidyl ether (TTE, Tech, PubChem CID: 103015) was purchased from Sigma-Aldrich. All other chemical reagents were of analytical grade.

2.2. Modification of Xanthan Gum

The modified XG was prepared in a four-necked flask equipped with a mechanical stirrer, a reflux condenser, a thermometer, and a N_2 gas inlet and outlet tube. The XG (1 g) was dissolved in 150 mL distilled water under constant stirring for

60 min at room temperature. Then, AM (15 g) and 260, 390, 520, 650 and 780 μL TTE were added into the XG solution sequentially and stirred, saturated with N_2 to remove dissolved oxygen. The temperature was held at 70°C, and 0.3 g of KPS was added and reacted for 4 h to initiate the graft copolymer. The modified XG was precipitated using ethanol. The precipitate was filtered, washed thoroughly with ethanol/water mixture (4:1, v/v) 3 times under high-speed stirring, and then soaked in an ethanol/water mixture (4:1, v/v) for 24 h. The modified XG was collected by filtration and dried at 50°C. Finally, the dried modified XG was ground and milled and then sieved through a 250 μm membrane. This was used as XGTTE. For the modified XG, TTE dosage of 260 μL (2%, w/w), 390 μL (3%, w/w), 520 μL (4%, w/w), 650 μL (5%, w/w) and 780 μL (6%, w/w) were recorded as XGTTE2, XGTTE3, XGTTE4, XGTTE5, and XGTTE6, respectively. We now provide some basic terminologies and notations that are necessary to understand the results. The percentage of grafting (G, %) and the percentage of monomer grafting (E, %) were calculated with equation (1) and (2), respectively.

$$G\ (\%) = (W_1\text{-}W_0)/W_0 \times 100\% \quad (1)$$

Here, W_0 is the weight in grams of the XG, W_1 is the weight in grams of XGTTE.

$$E\ (\%) = (W_1\text{-}W_0)/W_2 \times 100\% \quad (2)$$

Here, W_0 is the weight in grams of the XG, W_1 is the weight in grams of XGTTE, and W_2 is the weight in grams of the AM.

2.3. Crystal Violet Adsorption

The XGTTE (0.05 g) was transferred into 100 mL 30 mg/L CV with desired pH

and equilibrated for 24 h at 25°C. The CV was prepared by diluting the stock solution, which was prepared in distilled water. The aqueous solutions were decanted. The concentration of CV in the initial solution and the residual solutions were determined by recording the absorbance values at 590 nm. The equilibrium adsorption capacity (q_e, mg/g) was calculated with equation (3).

$$q_e = (C_i - C_e) \times V/m \quad (3)$$

Here, C_i is the initial CV concentration (mg/L), C_e is the residual CV concentration at equilibrium (mg/L), V is the volume of solution (L), and m is the amount of XGTTE (g) taken for adsorption measurements.

2.4. Flocculation Properties

The flocculation properties of XGTTE were investigated using an ultraviolet-visible spectrophotometer (T6, Beijing General Instrument Co., Ltd). The XGTTE (0.01 g) was added to 50 mL 5 g/L kaolin suspension liquid with constant stirring for 2 min at room temperature. This was allowed to stand for 10 min before being monitored via absorbance at 550 nm. The flocculation rate (Q, %) of XGTTE was calculated with equation (4).

$$Q\ (\%) = (A\text{-}B)/A \times 100\% \quad (4)$$

Here, A is the absorbance value of supernatant fluid of kaolin, and B is the absorbance value of the XGTTE sample.

2.5. Characterization of XGTTE

2.5.1. FT-IR Analysis

The FT-IR spectra of XGTTE and XG were recorded in solid state using KBr

pellets with a VERTEX 70 series FT-IR spectrometer (BRUKER OPTICS Co., GER) from 400 to 4000 cm^{-1} at 2 cm^{-1} resolution.

2.5.2. XRD Analysis

The structures of XGTTE and XG were investigated using Empyrean XRD instrument (Rigaku, Miniflex 600) with Cu Ka radiation source. The X-ray generator was operated at 40 kV and 15 mA; the reflection angle 2θ was monitored from 5 to 60° at a scanning speed of 10°/min and a step size of 0.02 (λ=1.5406 nm).

2.5.3. DSC Analysis

DSC measurements were carried out under N_2 flow (20 mL/min) using NETZSCH DSC 200F3 instruments from 45 to 500°C at a heating rate of 10°C/min. The sample mass was 14 mg.

2.5.4. Microstructure Analysis

The microstructure of XGTTE and XG were examined with a SEM (JSM-6380LV, JEOL), operating with secondary electrons under low vacuum at 15.0 kV. The samples were coated with Au prior to SEM examination.

The microscopic images were analyzed using Image J 1.42 q and plug-in FracLac-2.5 Release 1 d software programs according to Dàvila (Dàvila, Toldrà, Saguer, Carretero, & Parés, 2007). The fractal dimension (D_f) is based on the calculation of the scaling rule given by equation (5) and (6).

$$D = - \log N_\varepsilon / \log \varepsilon \quad (5)$$

Here, N_ε is the number of boxes at a certain scale containing part of the image, and ε is the corresponding scale.

Since the determination of D_f by image analysis is based on a two-dimensional space, it is necessary to add an extra dimension to the calculated D-value to represent the three-dimensional characteristics of the collagen system per equation (6).

$$D_f = D + 1 \quad (6)$$

The average pore diameter was calculated using equation (7) based on the threshold binary images with the public domain software ImageJ 1.42 q (Dàvila, Toldrà, Saguer, Carretero, & Parés, 2007).

$$d = \sqrt{4A/\pi} \quad (7)$$

Here, d is the average pore diameter, and A is the average pore area.

$$A = s \times k / n \quad (8)$$

Here, s is the total area of image, and k is the pore fraction.

3 Results and Discussion

3.1 Adsorption Capacity

The q_e of XGTTE2, XGTTE3, XGTTE4, XGTTE5, and XGTTE6 for CV are 28.13±0.528, 33.09±0.397, 35.12±0.820, 34.03±0.576, and 30.39±0.916 mg/g. These data were investigated at 25°C for 24 h, and the maximum q_e was 35.12±0.820 mg/g with XGTTE4. The q_e obtained here is somewhat higher than the Jalshakti polymer (12.90 mg/g) (Dhodapkar, Rao, Pande, Nandy, & Devotta, 2007), orange peel (14.30 mg/g) (Annadurai, Juang, & Lee, 2002) and coniferous pinus bark powder (32.78 mg/g) (Ahmad, 2009). Compared to the other materials like mino silica (40.00 mg/g) (Zhou, 2014), activated carbons (60.42 mg/g) (Senthilkumaar, Kalaamani, &

Subburaam, 2006), chitosan-graphite oxide-modified polyurethane (64.39 mg/g) (Qin, Qiu, Rong, Yan, Zhao, & Yang, 2015), and Nb_2O_5/SiO_2 (116.00 mg/g) (Umpierres, Prola, Adebayo, Lima, Dos Reis, Kunzler, et al., 2016), our method shows lower q_e values suggesting that the hydrogel developed here is a promising material for CV adsorption.

3.2. Flocculation Properties

The flocculation rate of XGTTE in a kaolin suspension liquid is shown in Table 1. The kaolin suspension was flocculated more efficiently with XGTTE. The maximum flocculation rate reached 85.63% with XGTTE2. As flocculation time proceeded, the flocculation rate of XGTTE increased and was over 90% within 24 h.

3.3. FT-IR Analysis

The FT-IR spectra of XG and XGTTE are shown in Fig. 1. There were no obvious changes in XGTTE2, XGTTE3, XGTTE4, XGTTE5, and XGTTE6. Some differences were observed in the spectra of XGTTE2 versus XG. The XG had a broad peak at 3443 cm^{-1} due to stretching vibrations of O-H group. The peak at 1730 cm^{-1} due to stretching vibrations of C=O. The peaks at 1624 cm^{-1} and 1414 cm^{-1} due to the asymmetrical and symmetrical vibrations of COO- groups. The peak at 1055 cm^{-1} was C_6-OH absorption.

The XGTTE2 had a broad peak at 3449 cm^{-1} due to stretching vibrations of O-H and N-H. The peaks at 1655 cm^{-1} and 1611 cm^{-1} are attributed to amide-I (the stretching vibrations of C=O) and amide-II (the bending vibrations of N-H) of the AM's amide group. Similar observations were also reported in cashew gum (Silva,

Paula, & Feitosa, 2007) and chitosan (Zhu, Yuan, Li, Yang, & Feng, 2004). The XGTTE2 had a peak at 1655 cm^{-1} due to the characteristic absorption of $CONH_2$, but the bending vibrations peak of C_6-OH at 1055 cm^{-1} decreased at XGTTE2. There are some new peaks in XGTTE2, and the peak at 1420 cm^{-1} is due to stretching vibrations of C-N. The peaks at 1117 cm^{-1} and 721 cm^{-1} are due to the wagging vibration of NH_2. In conclusion, these data confirmed the grafting of AM and TTE onto the XG.

3.4. XRD Analysis

XRD spectra of XG and XGTTE are shown in Fig. 2. There is a wide diffraction peak at 2θ=20.105˚showing the amorphous nature of XG, the crystalline interplanar spacing is 4.4129 nm. Similar results have also been reported by other authors (Chen, Chen, Chiou, Chen, Chen, & Fan, 2011). There is a wide diffraction peak roughly at 2θ=22˚of XGTTE. The 2θ of XGTTE2, XGTTE3, XGTTE4, XGTTE5 and XGTTE6 are 22.287˚, 21.890˚, 22.085˚, 22.281˚, and 22.474˚, respectively. The crystalline interplanar spacing of XGTTE2, XGTTE3, XGTTE4, XGTTE5, and XGTTE6 are 3.9855, 4.0570, 4.0215, 3.9867, and 3.9533 nm, respectively. Fig. 2 takes XGTTE4 and XGTTE6 for example. The crystalline interplanar spacing of XGTTE is smaller than that of XG. The peak width, peak intensity and the ratio of peak area to curve area of XGTTE4 and XGTTE6 were bigger than that of XG, suggesting that the crystalline state changed. The diffraction peak intensity of XGTTE increased with the increasing dosage of TTE and reached maximum at the dosage of 4% TTE. The TTE higher dosage decreased the diffraction peak intensity. Low levels of TTE can promote the crystallization of XGTTE, but high levels of TTE restrained the

crystallization of XGTTE. This then reduced the degree of crystallization of XGTTE. This suggested that AM and TTE changed the structure of XG. It could be inferred that the rearrangement in the morphology of the XGTTE strengthened the XG intra-molecular and inter-molecular hydrogen bond forces and improved the regularity of the molecular arrangements. This confirmed the success of hydrogel synthesis. This result is consistent with values obtained from the FT-IR spectra, which indicate that the chemical modifier reacts with -OH of XG and interferes with the regularity of the polymer chain making it difficult for XGTTE to crystallize.

3.5. Thermal Analysis

The DSC thermogram of XG and XGTTE are shown in Fig. 3. An endothermic curve within 50-70°C and an exothermic peak at 292.4°C were formed in the XG thermogram. The endothermal lower temperature and exothermal higher temperature are indicative of moisture loss and thermal decomposition of XG. Multiple endothermic peaks were observed in the thermal curve of XGTTE. The first broad endothermic peak is seen at 75-90°C and is due to loss of moisture. The melting of the XGTTE molecule occurs at 218.5°C and forms a second peak. Furthermore, the loss of ammonia exhibits a third peak at 330.1°C. The peak at 345°C resulted from the decomposition of the imide group formed via cyclisation. The last peak at 430°C represents decomposition of the cyclized imide groups. Similar observations were also reported during graft polymerization of AM onto cashew gum (Silva, Paula, & Feitosa, 2007). Thus, we concluded that the thermal stability of XG was improved by modification with AM and TTE.

3.6. SEM surface morphology

The morphological features of XG, XGTTE2, and XGTTE4 are shown in Fig. 4 and demonstrated that the microstructures of XGTTE were affected by TTE dose. The microstructure of the control group, XG, was less porous and more compact than XGTTE2 and XGTTE4. As TTE dose increased, the microstructure of the treated samples became more porous. The changes in surface morphology suggested graft copolymerization. This also supported in the FT-IR and XRD data.

To quantitatively describe the microstructure, the D_f and pore diameter were characterized. The D_f is a quantitative approach to measure pore characteristics and microstructure changes. The D_f value increased from 2.615 to 3.378 and d decreased from 5.701 to 2.756 μm as the dose of TTE increased from 2% to 4%, which resulted in a porous microstructure and higher D_f values. This was consistent with the SEM microstructure trend shown in Fig. 4, which confirmed increased porosity with higher TTE dose. Lacunarity is expressed as average pore diameter measurement complemented fractal analysis.

3.7. Mechanism of XGTTE Production

The XGTTE was prepared by graft copolymerization of AM onto XG in the presence of crosslinking agent TTE with KPS as a free radical initiator. Fig. 5 outlines the proposed mechanism for grafting and chemical crosslinking. During polymerization, the KPS initiator was decomposed under heating to generate sulfate anion-radicals. Sulfate radicals then reacted with the XG chain, breaking the ring structure of D-glucose in the XG resulting in the formation of more active groups

such as the alkoxy radicals. The FT-IR data showed that the bending vibrations peak of C_6-OH at 1055 cm^{-1} has a significant decrease at XGTTE indicating C_6-OH participation in reaction. Meanwhile, sulfate radicals attacked AM and TTE molecules, which led to the formation of AM and TTE-based radicals. Monomers of XG, AM, and TTE near the reaction site became acceptors of radicals resulting in chain initiation; they thereafter became free radical donors to neighboring molecules, which caused the graft chain to grow indefinitely. The polymer chains reacted with the end vinyl groups of the cross-linker, TTE, during chain propagation. The main chain of XG was then extended with the reaction between the hydroxyl groups of XG react with AM. The TTE was connected to the polymer chain and become the cross-linking point because the amino of AM and the epoxy of TTE showed a ring-opening reaction upon heating. The copolymer was comprised of a cross-linked and network structure that gradually formed XGTTE.

Table 1 summarizes the formulation details used in the synthesis. The percentage of grafting varied from 1584 to 1976, and the percentage of monomer grafting varied from 106 to 132. This is about 2 to 4 times of the graft copolymer synthesized by Raghavendra et al. (Mundargi, Patil, & Aminabhavi, 2007).

4. Conclusions

XG was grafted with AM and TTE, and it promotes higher regularity, better thermally stability, and a more porous structure. That resulted in the adsorption of crystal violet and kaolin flocculation. And XGTTE synthesized from 4% TTE displayed the maximum value of q_e. The results implied that XGTTE could be an

effective adsorbent for removal of CV from aquaculture water and contribute to the production of healthy food.

Acknowledgments

We gratefully acknowledge the financial support from the projects: KXGH17001, C200402, and 2018I0101. We thank LetPub (www.letpub.com) for its linguistic assistance during the preparation of this manuscript.

Reference

Aflaki, J. M., Dadvand, K. A., & Sheykhan, M. (2016). Experimental study of the removal of copper ions using hydrogels of xanthan, 2-acrylamido-2-methyl-1-propane sulfonic acid, montmorillonite: Kinetic and equilibrium study. *Carbohydrate Polymers, 142*, 124-132.

Ahmad, R. (2009). Studies on adsorption of crystal violet dye from aqueous solution onto coniferous pinus bark powder (CPBP). *Journal of Hazardous Materials, 171*(1-3), 767-773.

Annadurai, G., Juang, R. S., & Lee, D. J. (2002). Use of cellulose-based wastes for adsorption of dyes from aqueous solutions. *Journal of Hazardous Materials, 92*(3), 263-274.

Ashraf, W. (2005). Accumulation of heavy metals in kidney and heart tissues of epinephelus microdon fish from the arabian gulf. *Environmental Monitoring & Assessment*, 101(1-3):311-316.

Aysu, T., & Küçük, M. M. (2015). Removal of crystal violet and methylene blue from aqueous solutions by activated carbon prepared from Ferula orientalis. *International Journal of Environmental Science and Technology*, *12*(7), 2273-2284.

Behari, K., Pandey, P. K., Kumar, R., & Taunk, K. (2001). Graft copolymerization of acrylamide onto xanthan gum. *Carbohydrate Polymers*, *46*(2), 185-189.

Bhardwaj, T. R., Kanwar, M., Lal, R., & Gupta, A. (2000). Natural gums and modified natural gums as sustained-release carriers. *Drug Development and Industrial Pharmacy*, *26*(10), 1025-1038.

Biswas, A., Pal, S., & Udayabhanu, G. (2015). Experimental and theoretical studies of xanthan gum and its graft co-polymer as corrosion inhibitor for mild steel in 15% HCl. *Applied Surface Science*, *353*, 173-183.

Chen, C. C., Chen, W. C., Chiou, M. R., Chen, S. W., Chen, Y. Y., & Fan, H. J. (2011). Degradation of crystal violet by an FeGAC/H_2O_2 process. *Journal of Hazardous Materials*, *196*(12), 420-425.

Dàvila, E., Toldrà, M., Saguer, E., Carretero, C., & Parés, D. (2007). Characterization of plasma protein gels by means of image analysis. *LWT-Food Science and Technology*, *40*(8), 1321-1329.

Dhodapkar, R., Rao, N. N., Pande, S. P., Nandy, T., & Devotta, S. (2007). Adsorption of cationic dyes on Jalshakti, super absorbent polymer and photocatalytic regeneration of the adsorbent. *Reactive and Functional Polymers*, *67*(6), 540-548.

Ding, W., Yiming, H. A., Yanjie, L. I., Bao, Y., & Yongfu, L. I. (2016). Synthesis and structural properties of xanthan gum-g-N-vinylpyrrolidone graft copolymer prepared by radiation. *Journal of Nuclear Agricultural Sciences*, *30*(4), 695-703.

Gils, P. S., Ray, D., & Sahoo, P. K. (2009). Characteristics of xanthan gum-based biodegradable superporous hydrogel. *International Journal of Biological Macromolecules*, *45*(4), 364-371.

Huang, B., Huang, S., Shi, Y., & Mo, J. (2005). Synthesis of a novel photosensitive prepolymer with trimethylolpropane triglycidylether and acrylic acid as starting materials. *Journal of Wuhan University of Technology-Mater. Sci. Ed.*, *20*(2), 29-31.

Huang, X., Wang, Y., Liao, K., &Yuan, D. (2015). Simultaneous determination of malachite green, crystal violet and their leuco-metabolites in aquaculture water samples using monolithic fiber-based solid-phase microextraction coupled with high performance liquid chromatography. *Analytical Methods*, 7(19):8138-8145.

Katzbauer, B. (1998). Properties and applications of xanthan gum. *Polymer Degradation & Stability*, *59*(1-3), 81-84.

Kumar, A., Singh, K., & Ahuja, M. (2009). Xanthan-g-poly(acrylamide): microwave-assisted synthesis, characterization and in vitro release behavior. *Carbohydrate Polymers*, *76*(2), 261-267.

Lee, J. B., Kim, H. Y., Jang, Y. M., Song, J. Y., Woo, S. M., Park, M. S., Lee, H. S., Lee, S. K., & Kim, M. (2010). Determination of malachite green and crystal violet in processed fish products. *Food Additives & Contaminants Part A Chemistry Analysis Control Exposure & Risk Assessment*, 27(7):953-961.

Lin, Y., He, X., Han, G., Tian, Q., & Hu, W. (2011). Removal of crystal violet from aqueous solution using powdered mycelial biomass of *Ceriporia lacerata* P2. *Journal of Environmental Sciences*, *23*(12), 2055-2062.

Mahdavinia, G. R., Aghaie, H., Sheykhloie, H., Vardini, M. T., & Etemadi, H. (2013). Synthesis of CarAlg/MMt nanocomposite hydrogels and adsorption of cationic crystal violet. *Carbohydrate Polymers*, *98*(1), 358-365.

Mani, S., Bharagava, R. N. (2016). Exposure to crystal violet, its toxic, genotoxic and carcinogenic effects on environment and its degradation and detoxification for environmental safety. *Reviews of Environmental Contamination & Toxicology*, 237(12):71-104.

Monash, P., & Pugazhenthi, G. (2009). Adsorption of crystal violet dye from aqueous solution using mesoporous materials synthesized at room temperature. *Adsorption*, *15*(4), 390-405.

Mundargi, R. C., Patil, S. A., & Aminabhavi, T. M. (2007). Evaluation of

acrylamide-grafted-xanthan gum copolymer matrix tablets for oral controlled delivery of antihypertensive drugs. *Carbohydrate Polymers, 69*(1), 130-141.

Pal, A., Majumder, K., & Bandyopadhyay, A. (2016). Surfactant mediated synthesis of poly(acrylic acid) grafted xanthan gum and its efficient role in adsorption of soluble inorganic mercury from water. *Carbohydrate Polymers, 152*, 41-50.

Pal, A., Pan, S., & Saha, S. (2013). Synergistically improved adsorption of anionic surfactant and crystal violet on chitosan hydrogel beads. *Chemical Engineering Journal, 217*(22), 426-434.

Pandey, S., & Mishra, S. B. (2011). Graft copolymerization of ethylacrylate onto xanthan gum, using potassium peroxydisulfate as an initiator. *International Journal of Biological Macromolecules, 49*(4), 527-535.

Qin, J., Qiu, F., Rong, X., Yan, J., Zhao, H., & Yang, D. (2015). Adsorption behavior of crystal violet from aqueous solutions with chitosan–graphite oxide modified polyurethane as an adsorbent. *Journal of Applied Polymer Science, 132*(17), 83-101.

Sahoo, C., Gupta, A. K., & Pal, A. (2005). Photocatalytic degradation of crystal violet (C.I. Basic Violet 3) on silver ion doped TiO_2. *Dyes and Pigments, 66*(3), 189-196.

Senthilkumaar, S., Kalaamani, P., & Subburaam, C. V. (2006). Liquid phase adsorption of crystal violet onto activated carbons derived from male flowers of coconut tree. *Journal of Hazardous Materials, 136*(3), 800-808.

Silva, D. A. D., Paula, R. C. M. D., & Feitosa, J. P. A. (2007). Graft copolymerisation of acrylamide onto cashew gum. *European Polymer Journal, 43*(6), 2620-2629.

Umpierres, C. S., Prola, L. D., Adebayo, M. A., Lima, E. C., Dos Reis, G. S., Kunzler, D. D.,

Dotto, G. L., Arenas, L. T., & Benvenutti, E. V. (2016). Mesoporous Nb_2O_5/SiO_2 material obtained by sol-gel method and applied as adsorbent of crystal violet dye. *Environmental Technology, 38*(5), 566-578.

Xiong, Y., Zhang, X., & Liu, M. Z. (2015). Surface-crosslinked guar gum-g-sodium polyacrylate superabsorbents: swelling characteristics and mechanics performance. *Applied Mechanics and Materials, 729*, 39-46.

Zhou, D. (2014). Adsorption of crystal violet onto amino silica: optimization, equilibrium, and kinetic studies. *Desalination and Water Treatment, 52*(31), 6113-6121.

Zhu, L., Yuan, M., Li, W., Yang, Y., & Feng, Z. (2004). Synthesis and flocculation property of chitosan-acrylamide graft copolymer. *Chemical Research in Chinese Universities*, *20*(2), 221-224.

Figure caption:

Fig. 1 The FT-IR spectra of XG, XGTTE2, XGTTE3, XGTTE4, XGTTE5 and XGTTE6 from 4000-400 cm^{-1}.

Fig. 2 X-ray diffraction spectra of XG (black line), XGTTE4 (red line) and XGTTE6 (blue line). The X-ray generator was operated at 40 kV and 15 mA. The XRD chromatograms were recorded over an angular range of 5° to 60° (2θ) at a scanning speed of 10°/min and a step size of 0.02 (λ=1.5406 nm).

Fig. 3 DSC curves of XG (black line), XGTTE2 (red line), XGTTE3 (blue line), XGTTE4 (rose red line), XGTTE5 (green line) and XGTTE6 (purple line) from 45-500°C at a heating rate of 10°C/min under N_2 flow (20 mL/min).

Fig. 4 SEM micrograph of XGTTE2, XGTTE4 and XG at 3000× and 1000×: (a)

XGTTE2; (b) XGTTE4; (c) XG; (d) XGTTE2; (e) XGTTE4; and (f) XG. SEM analyses were performed using a JSM-6380LV (JEOL) operated with an accelerating voltage of 15.0 kV. The samples were coated with Au prior.

Fig. 5 The mechanism of XGTTE uses TTE as a cross-linker. Sulphate radicals were generated under heating, and the sulphate radical abstracts hydrogen atoms from the XG molecules producing XG free radicals. The monomer molecules, which are in close vicinity to the reaction sites, become acceptors of the XG radicals resulting in chain initiation. Thereafter, they become free radical donors to the neighboring molecules causing the grafted chains to grow.

Table 1

The synthetic details and flocculation rate of XGTTE.

Code	Wt. of XGTTE (g) *	*G* (%)*	*E* (%)*	*Q* (%)*
XGTTE2	19.5213±0.0054c	1850.8900±0.9557c	123.4467±0.0410b	85.6300±0.0173a
XGTTE3	20.0751±0.0025d	1898.1267±2.2478b	127.0767±0.0644ab	43.6133±0.0555e
XGTTE4	16.9365±0.0260e	1588.5933±3.9657e	106.1933±0.1906c	84.3600±0.0872b
XGTTE5	17.0826±0.0054b	1607.2333±0.5266d	111.6200±4.4200c	62.5667±0.2505c
XGTTE6	20.755±0.0278a	1974.4633±3.0082a	131.6900±0.1828a	61.6000±0.2082d

Values in the Wt. of XGTTE, *G*, *E* and *Q* column followed by letters are significantly different ($p<0.05$).

*Values are mean ±SD of duplicate runs.

Highlights:

- Xanthan gum was grafted with acrylamide and trimethylolpropane triglycidyl ether
- The grafted xanthan gum indicated a porous honeycomb-like structure.
- The grafted xanthan gum was evaluated as an adsorbent to remove crystal violet.
- The thermal stability of the grafted xanthan was improved.

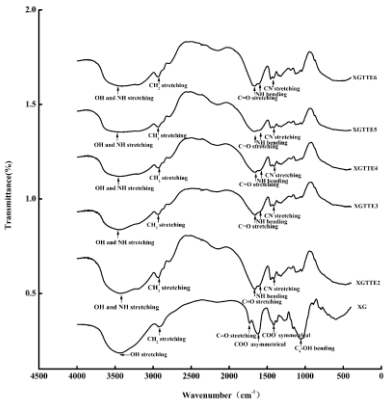

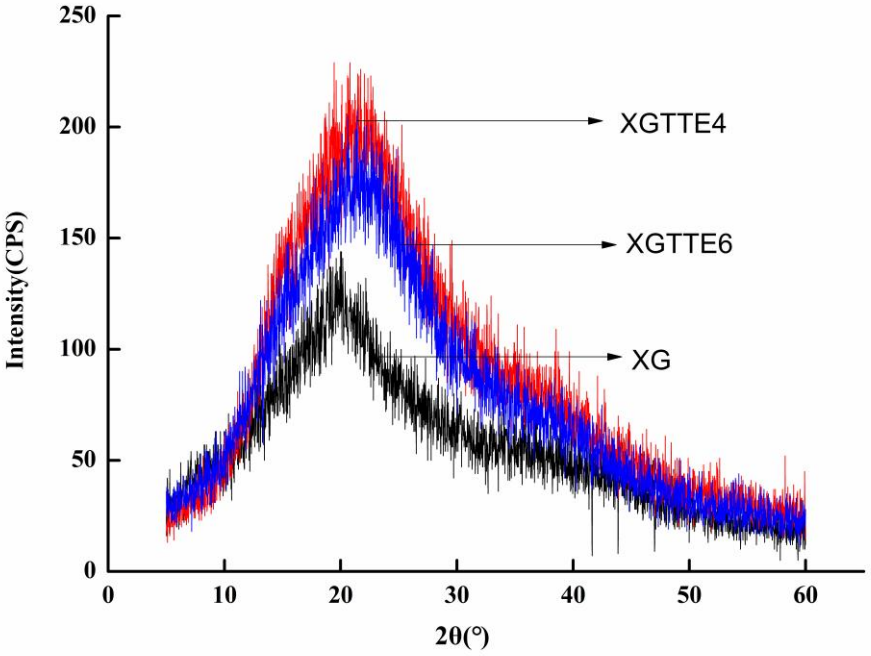

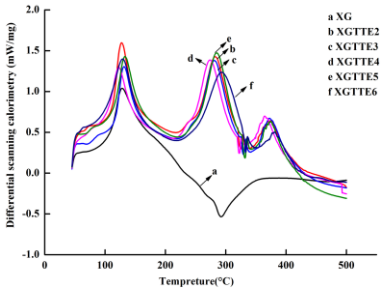

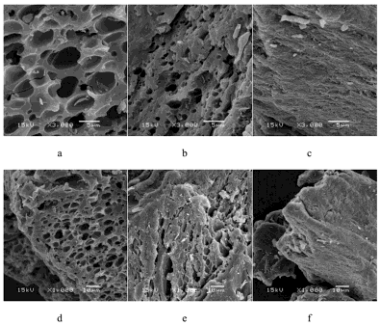

a b c

d e f

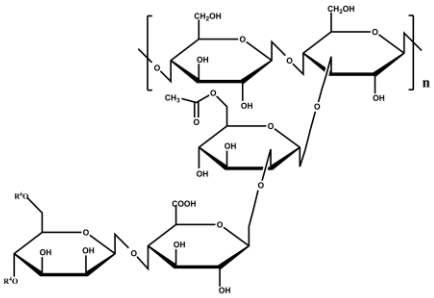

=

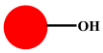

XG

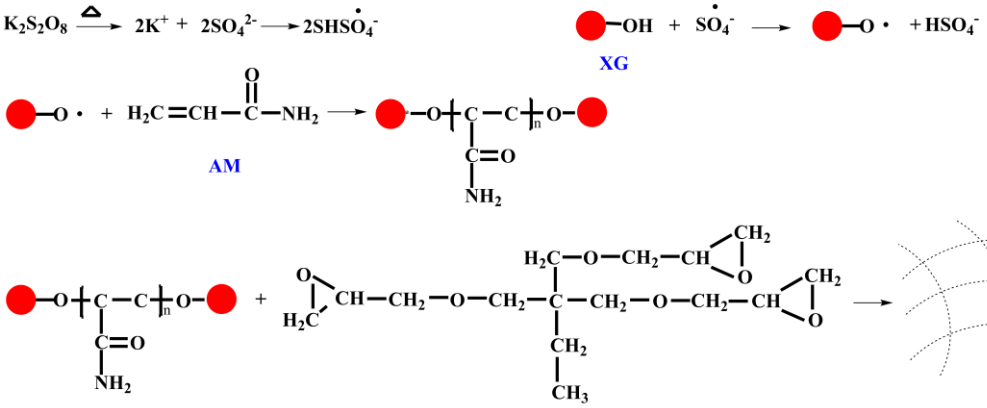

XG

AM

TTE

XGTTE